

DETECTION OF COLLAPSED BUILDINGS DUE TO THE 2016 KUMAMOTO EARTHQUAKE FROM LIDAR DATA

Luis MOYA⁽¹⁾, Fumio YAMAZAKI⁽²⁾, Wen LIU⁽³⁾, Tatsuro CHIBA⁽⁴⁾, Erick MAS⁽⁵⁾

⁽¹⁾ Postdoctoral researcher, International Research Institute of Disaster Science, Tohoku University, Japan,
lmoyah@irides.tohoku.ac.jp

⁽²⁾ Professor, Department of Urban Environment Systems, Chiba University, Japan, fumio.yamazaki@faculty.chiba-u.jp

⁽³⁾ Assistant professor, Department of Urban Environment Systems, Chiba University, Japan,
wen.liu@faculty.chiba-u.jp

⁽⁴⁾ Research and Development Institute, Asian Air Survey Co., Ltd., Kawasaki 215-0044, Japan, ta.chiba@ajiko.co.jp

⁽⁵⁾ Associate Professor, International Research Institute of Disaster Science, Tohoku University, Japan,
mas@irides.tohoku.ac.jp

...

Abstract

On April 14, 2016 at 21:26, an Mw 6.5 earthquake occurred in Kumamoto prefecture, Japan. Soon after, about 28 hours later, another earthquake of Mw 7.1 occurred. Thus, the first event was designated as the foreshock and the second one as the mainshock. The both epicenters were located close to residential areas, such as Mashiki town, Kashima town, Mifune town and Nishihara village. Therefore, the earthquake produced extensive losses to the infrastructure and human losses. In this paper, building collapsed and landslide produced during the mainshock are detected from a pair of digital surface models (DSM), before and after the mainshock, obtained from airborne Lidar data. Based on the difference of the building height between the pre-event DSM and post-event DSM, the collapsed buildings and undamaged buildings are recognized. Our results point out that Lidar technology is an important tool in disaster management.

Keywords: Lidar, the 2016 Kumamoto earthquake, building damage

1. Introduction

On April 14, 2016 at 21:26, an Mw6.5 earthquake occurred in Kumamoto prefecture, Japan. The epicenter (32.7°N, 130.8°E and 11 km depth) was located at the end of the Hinagu fault. About 28 hours later (April 16, 2016 at 01:25), another earthquake of Mw7.1 occurred in the Futagawa fault. Thus the first event was designated as the "foreshock" and the second one as the "mainshock". The both events were located in the suburban area of Kumamoto city with 735 thousand population. Therefore, extensive damage such as human loss, collapse of buildings and bridges, landslides, damage to soils and foundations, and damage of historical structures occurred.

Collapse of buildings during earthquakes is the main cause of human loss and thus it is important to quantify the collapsed buildings for disaster loss assessment. Remote sensing technologies are very useful for this purpose (Yamazaki and Matsuoka, 2007; Yamazaki and Liu, 2016) because it provides a rapid estimation of the degree of damage produced by earthquakes. Based on the sensor type, remote sensing technologies can be categorized in two types (Yamazaki and Liu, 2016): passive, which includes optical and thermal sensors, and active, such as Synthetic Aperture Radar (SAR) and Light Detection and Ranging (Lidar).

In this paper we will explore the potential use of Lidar data to extract collapsed buildings during the mainshock of the 2016 Kumamoto earthquake. Lidar data have the advantage that it can provide geometrical features of buildings (Vu et al., 2003; Vu et al., 2009); although efforts have been made to extract building features from other sensors (Liu et al., 2014; Suzuki et al., 2014; Zakeri et al., 2015). We used two DSMs (Digital Surface Model), before and after the earthquake, obtained from Lidar data and extract the elevation inside the buildings footprint data. Three parameters are used: an average of the difference of the elevations, the standard deviation of the differences of elevation, and the standard deviation of pre-event DSM and post-event DSM. Then, the K-mean cluster method is applied to separate collapsed buildings from un-collapsed ones. The result represents a preliminary attempt to grasp collapsed buildings and it will contribute to improve a better framework that will be published later.

2. The study area and data

On April 15, 2016, one day after the big foreshock, a Lidar DSM was collected by Asia Air Survey Co., Ltd. The survey generated the DSM with the ground return density averaging 1.5~2 points/m². Soon after, a second mission was sent on April 23 because of the un-expected mainshock occurred on April 16. The second mission generated DSM with the average point density of 3~4 points/m². This dataset is one of the few cases in which pre- and post-event DSMs are available with the same airplane, instrument and pilot (Air Survey Co., Ltd., 2016). For the sake of brevity, the DSM collected on April 15 and April 23 will be referred as PreDSM and PostDSM, respectively. After rasterize the raw point clouds, the DSMs have a data spacing of 50 cm.

Fig. 1 shows the extension of the PreDSM and PostDSM, where it can be observed that the PreDSM extends a bigger area than the PostDSM does. The common area from the both DSMs covers parts of the Mashiki town, Kashima town, Mifune town, and Nishihara village. The whole common area is composed of rural residential areas, agricultural fields and forests. The common area also includes a part of the Futagawa fault, which caused the mainshock of the Kumamoto earthquake.

Since the study area is located close to the epicenter and the active Futagawa fault, a permanent crustal deformation was produced during the earthquake. Therefore, it is necessary to consider this shift in the PostDSM before detecting the collapsed building. An automatic procedure to calculate the three-dimensional permanent deformation was implemented by Moya et al. (2016) and applied to these Lidar data. **Fig. 2** illustrates the east-west and north-south components of the permanent displacement occurred during the Kumamoto earthquake. The horizontal deformation of up to 2 m and the subsidence of up to 2 m were observed in the study area. As mentioned before, the post-event DSM was shifted by the direction and magnitude of the permanent crustal deformation. Then, the detection of collapsed buildings is carried out and shown in the next section.

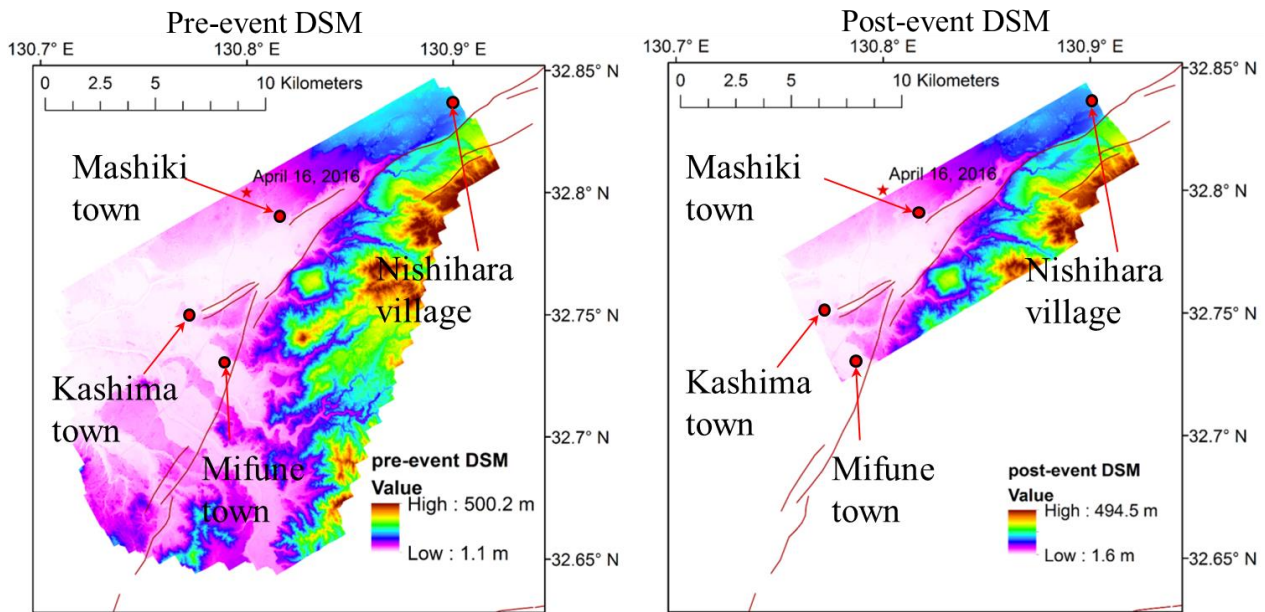


Fig. 1- DSMs acquired before and after the 2016 Mw 7.1 Kumamoto earthquake (Modified from Moya et al., 2016).

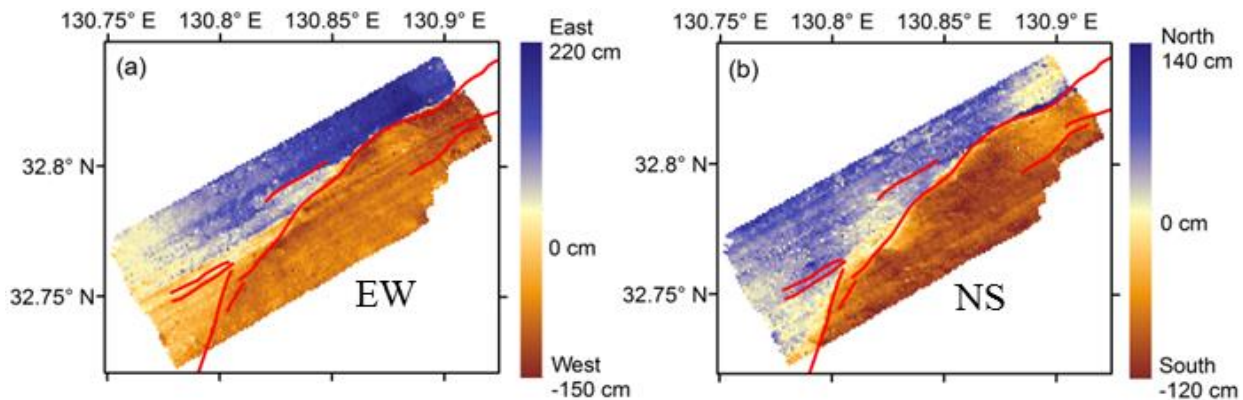


Fig. 2- Horizontal components of the permanent displacement occurred during the 2016 Mw 7.1 Kumamoto earthquake within the study area (Modified from Moya et al. 2016).

3. Extraction of collapsed buildings

Fig. 3 shows the elevation of two buildings: a collapsed building and an uncollapsed one. The blue and red dots represent the elevation recorded before and after the earthquake, respectively. There is a clearly reduction of the elevation in the case of the collapsed building in comparison with the uncollapsed building. Therefore, the difference between the elevations before and after the earthquake is used as a parameter to extract collapsed buildings. To simplify the evaluation, the average of the difference within the footprint area of a building is used (*DIF*). Additionally, two more parameters are used to evaluate the buildings: the standard deviation (*STD*) of the differences of elevations and the correlation coefficient (*r*) between the elevations of the PreDSM and PostDSM. The standard deviation is used to consider partially collapsed buildings, which would show higher standard deviations compared with those of undamaged or totally collapsed buildings. The correlation coefficient (*r*) has proved to be effective to detect changes between a pair of satellites images (Upreti et al., 2013; Liu et al., 2013). The *r* ranges from -1 to 1 and basically if *r* is close to one, it is assumed that there is no change and if *r* is close to zero it is assumed that a change occurred. Therefore, the three parameters are calculated for each building as follows:

$$DIF = \frac{1}{N} \sum_{i=1}^N (Ha_i - Hb_i) \quad (1)$$

$$STD = \sqrt{\frac{\sum_{i=1}^N ((Ha_i - Hb_i) - DIF)^2}{N}} \quad (2)$$

$$r = \frac{N \sum_{i=1}^N Ha_i Hb_i - \sum_{i=1}^N Ha_i \sum_{i=1}^N Hb_i}{\sqrt{\left(N \sum_{i=1}^N Ha_i^2 - \left(\sum_{i=1}^N Ha_i \right)^2 \right) \cdot \left(N \sum_{i=1}^N Hb_i^2 - \left(\sum_{i=1}^N Hb_i \right)^2 \right)}} \quad (3)$$

where $i \in \{1, 2, \dots, N\}$ is the sub-index that represent the i -th location inside a building-footprint area. N is the number of elevations inside a building footprint. Ha_i and Hb_i are the elevations obtained from the PreDSM and PostDSM, respectively. The building-footprint information is provided by the Geospatial Information Authority of Japan (GSI). We evaluate only buildings with footprint areas of more than 20 m². The parameters of the buildings shown in **Fig. 3** are depicted in **Table 1**. As you can see, the DIF and r show a clear contrast between the two buildings. It means, low r and high DIF for the collapsed building and the opposite for the undamaged building. On the other hand, STD does not show a big difference between the collapsed and undamaged buildings. From a closer look, three main reasons produce the high STD in undamaged buildings. First, the resolution of the average point density might produce some differences in the edges of the buildings. Secondly, there is not a precise matching between the Lidar data and the building-footprint database. Thus, some surrounding ground elevation data are also included in the calculation, which may be increased by a neighboring collapsed-building. Thirdly, a building could suffer from a slight lateral distortion that makes some elevation points at the boundary of the footprint polygon change considerably.

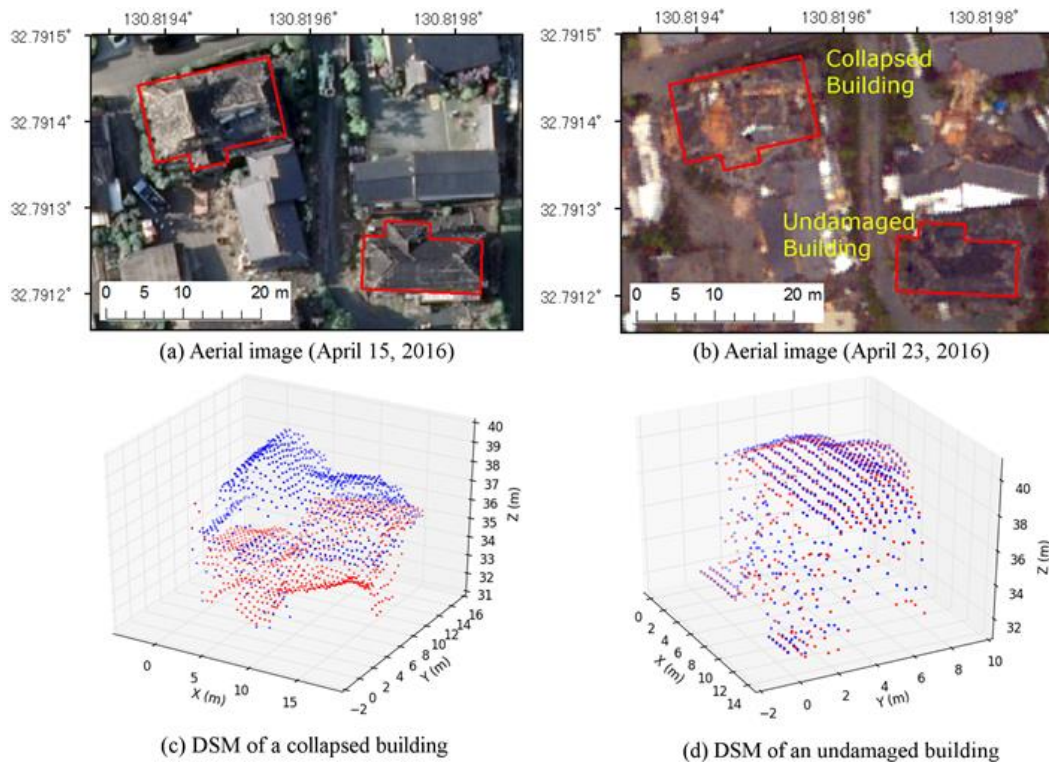


Fig. 3- The aerial images taken before (a) and after (b) the earthquake and the DSMs of a collapsed and un-collapsed building (c and d). The blue dots represent the PreDSM and the red dots the PostDSM

Table 1- Control parameters (*DIF*, *STD*, and *r*) of the two buildings shown in Fig. 3

| building | DIF | STD | R |
|-----------|-------|------|------|
| Collapsed | -2.85 | 1.64 | 0.07 |
| Undamaged | -0.09 | 1.04 | 0.91 |

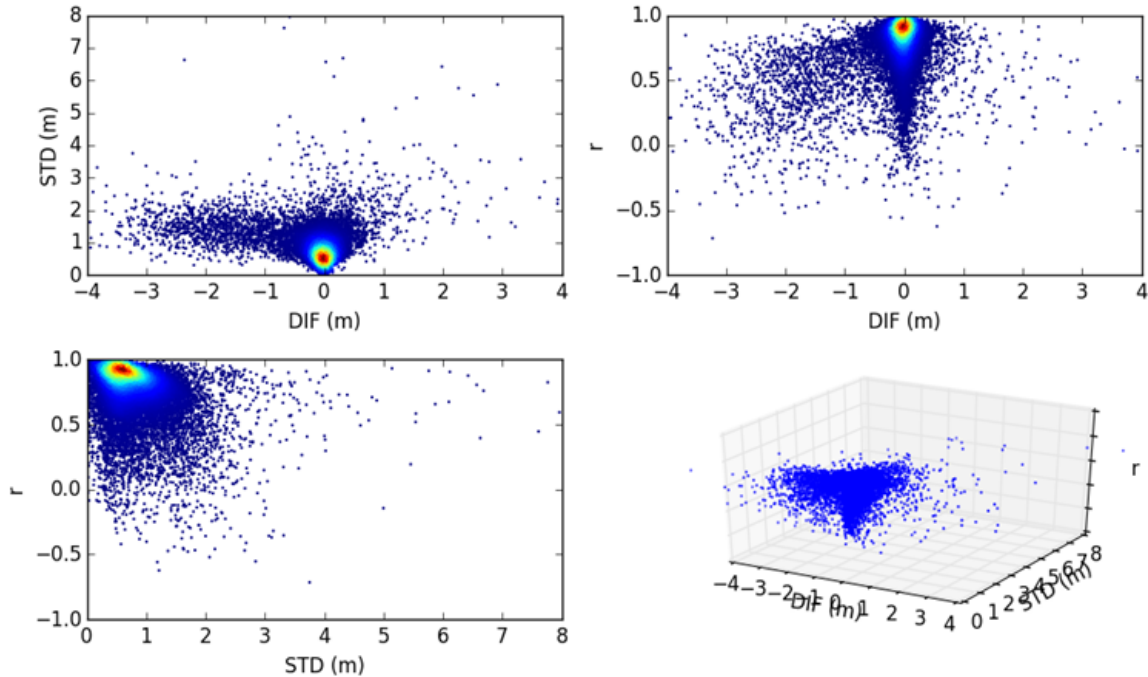


Fig. 4- Scatter plot of the parameters used for the detection of collapsed buildings

A total of 26,071 building were evaluated. First we extracted the elevations of the points inside each building and then the *DIF*, *STD* and *r* were calculated. **Fig. 4** shows the parameters calculated for each building where the shaded color depicts the density of the dots. As can be seen, most of the points are located at approximately $(DIF, STD, r) = (0 \text{ m}, 0.5 \text{ m}, 0.9)$ which represent indeed undamaged buildings. The next issue is the criterion to set a threshold that could separate properly collapsed buildings. It is obvious that the buildings that have the lowest values of *DIF* represent collapsed buildings. What is not clear is to establish the value that would be used to judge which buildings are collapsed. Here, the K-mean cluster method is used to extract collapsed buildings. The method clusters the data and separates them into a specified number of sets. The objective of the method is to minimize the inertia of each set:

$$\min \sum_{i=1}^k \sum_{x \in S_i} \|x - \mu_i\|^2 \quad (4)$$

where for our purpose, x is a vector that contains the control parameters (*DIF*, *STD*, *r*), $k = 2$ is the number of sets: collapsed and uncollapsed buildings, S_i represent a specific set, and μ_i is the centroid of a set S_i . Additional details on this method can be found in Alpaydin (2014). The first step of the method is a first estimation of the centroid of each set and groups all the data to the closest centroid. Then, a looping process is applied to update the location of the centroid based on the average of the samples of each set. The loop stops when the centroid does not move longer that certain threshold. **Fig. 5** shows the groups of data obtained from the K-mean cluster method. It is observed a clear threshold in the *DIF* parameter with a value of approximately -1m (**Fig. 5a-b**). On the other hand, there is not threshold for the other two parameters. These results at least show that *DIF* is the key parameter.

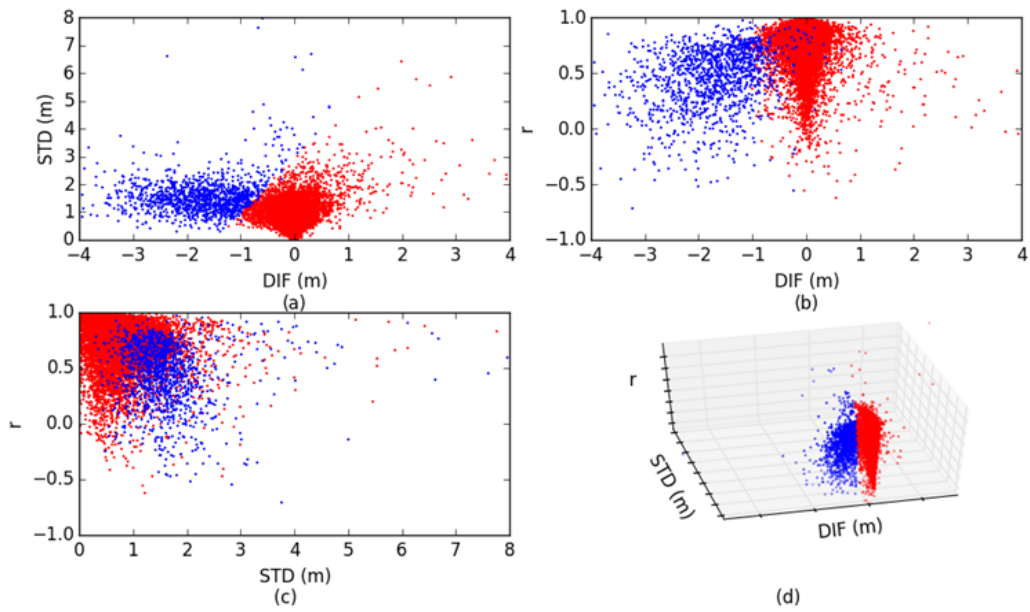


Fig. 5- Classification of uncollapsed and collapsed buildings by the K-mean cluster method.

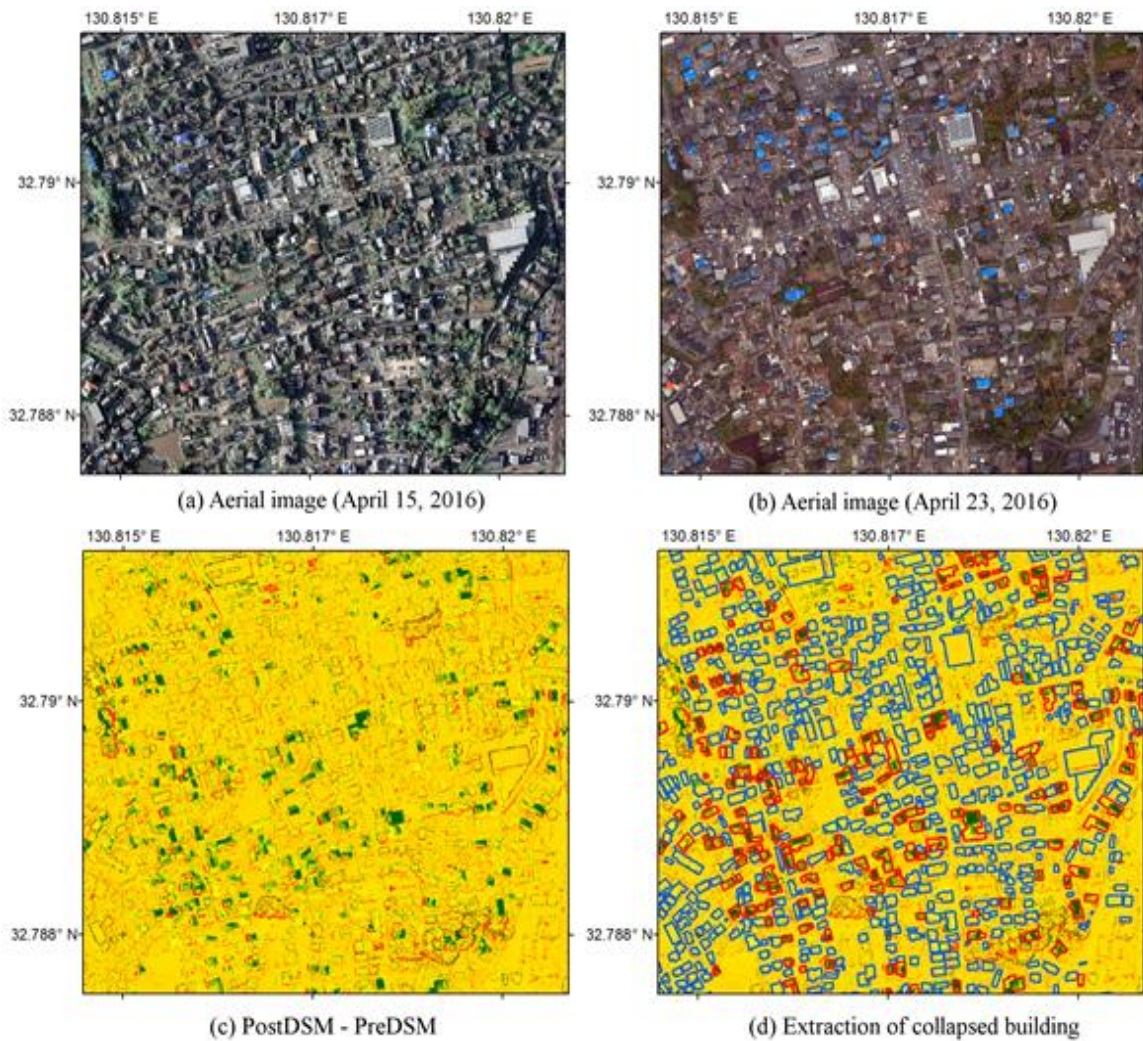


Fig. 6- Spatial distribution of collapsed buildings inside an area of Mashiki town.

In order to evaluate the result from the K-means cluster method, a zooming up of an area in Mashiki town, which is one of the most severely damaged areas, is shown in **Fig. 6**. The aerial images taken before and after the earthquake, which have a resolution of 16 cm and 25 cm, are shown in **Fig. 6a** and **6b**, respectively. The difference of elevation between the PostDSM and PreDSM is shown in **Fig. 6c**. The dark green pixels represent high negative values, while dark red pixels represent high positive values. When the dark green pixels are cluster, there is high possibility that those represent a collapsed building. Besides, it can be observed also either green or red values aligned forming polygons. Those, lines are due to the imperfect matching of building-elevation values between the PreDSM and the PostDSM. As mentioned before, those pixel values produced high values of STD.

Fig. 6d shows an overlapping of the collapsed buildings extracted from the K-means cluster method with the differences of DSMs (**Fig. 6c**). The red polygons are the building-footprints that were classified as collapsed, while the blue polygons represent uncollapsed buildings. The automatic extraction shows consistency with visual inspection of the collapsed buildings that can be performed from **Fig. 6c**. From the 26,071 buildings that were evaluated, 1,300 buildings were classified as collapsed.

4. Conclusions

An automatic procedure to extract collapsed buildings from a pair of Lidar data taken before and after the 2016 Kumamoto earthquake was performed. For this purpose, the geographic information of building-footprints was employed, which was provided by the government. Three parameters were selected to evaluate if a buildings collapsed or not: the average of the differences between the PreDSM and PostDSM data within a building footprint (DIF), the standard deviation of that differences (STD), and the correlation coefficient between the PreDSM and PostDSM (r). The K-mean cluster method was selected to define two sets of data: collapsed and uncollapsed buildings. From the results, it was observed that DIF was the main parameter to distinguish the collapsed buildings. From a total of 26,071 evaluated buildings, the method extracted 1,300 collapsed buildings. The results were compared with an area within the Mashiki town and showed a good agreement from a visual inspection evaluation. However, a deeper evaluation of the results (i.e., a comparison with field survey data and a look of the overall results) is necessary.

It was also observed that in order to improve the quality of the parameters, it is recommended to discard the elevation points located at the boundaries of building footprint polygons because there is not a perfect matching between the PreDSM and the PostDSM and this fact increases considerably the STD. These preliminary results are helpful to provide an idea of where are concentrating the collapsed buildings. However, as mentioned before, it is necessary a deep evaluation of the results. What is also important is to define properly the relation between the parameters used (DIF , STD , r) and the typology of the collapsed buildings. All this points will be addressed in the final publication of this research.

5. Acknowledgements

The LIDAR data and aerial photographs used in this study were acquired and owned by Asia Air Survey Co., Ltd., Japan.

6. References

- [1] Alpaydin, E. (2014): Introduction to machine learning, Third Edition, *The MIT press*, Cambridge.
- [2] Asia air Survey Co., Ltd.: The 2016 Kumamoto Earthquake. <http://www.ajiko.co.jp/en/blog/y2016/id572751JWX/> (last accessed August 2016).
- [3] Liu, W., Yamazaki, F., Gokon, H., and Koshimura, S. (2013): Extraction of tsunami-flooded areas and damaged buildings in the 2011 Tohoku-Oki earthquake from Terra-SAR intensity images. *Earthquake Spectra*, Vol. 29, No. S1, S183-S200.

- [4] Liu, W., Yamazaki, F., Adriano, B., Mas, E., Koshimura, S. (2014): Development of building height data in Peru from high-resolution SAR imagery. *Journal of Disaster Research*, Vol. 9, No. 6, pp. 1042-1049.
- [5] Maruyama, Y., Tashiro, A., and Yamazaki, F. (2014): Detection of collapsed buildings due to earthquakes using a digital surface model constructed from aerial images. *Journal of Earthquake and Tsunami*, Vol. 8, No. 1, 13 p.
- [6] Moya, L., Yamazaki, F., Liu, W., and Chiba, T. (2016): Calculation of coseismic displacement from Lidar data in the 2016 Kumamoto, Japan, earthquake. *Nat. Hazards Earth Syst. Sci. Discuss.*, doi:10.5194/nhess-2016-315, in review.
- [7] Suzuki, K., Liu, W., and Yamazaki, F. (2014): Height estimation of buildings from high-resolution SAR data based on interferometric analysis. *Proc. 35th Asian Conference on Remote Sensing*, Nay Pyi Taw, Myanmar, 6 p.
- [8] Uprety, P., Yamazaki, F. (2013): Damage detection using high-resolution SAR imagery in the 2009 L'Aquila, Italy, earthquake. *Earthquake Spectra*, Vol. 29, No. 4, pp 1521-1535.
- [9] Vu, T. T., Tokunaga, M., and Yamazaki, F. (2003): Wavelet-based extraction of building features from airborne laser scanner data. *Can. J. Remote Sensing*, Vol. 29, No. 6, pp. 783-791.
- [10] Vu, T. T., Yamazaki, F., and Matsuoka, M. (2009): Multi-scale solution for building extraction from LiDAR and image data. *International Journal of Applied Earth Observation and Geoinformation*, Vol. 11, 281-289.
- [11] Yamazaki, F., and Matsuoka, M. (2007): Remote sensing technologies in post-disaster damage assessment. *Journal of Earthquakes and Tsunamis*, Vol. 1, No. 3, pp 193-210.
- [12] Yamazaki, F., and Liu, W. (2016): Remote sensing technologies for post-earthquake damage assessment: A case study on the 2016 Kumamoto earthquake. Keynote Lecture, 6th ASIA Conference on Earthquake Engineering, Cebu city, Philippines, 8 p.
- [13] Zakeri, H., Liu, W., Yamazaki, F., Nonaka, T., and Sasagawa, T. (2015): Building damage assessment in the 2010 Haiti earthquake using high resolution SAR imagery. *Proc. of the International Symposium on Remote Sensing, Tainan, Taiwan*, 4 p.